Deciphering the selectivity of CBL-B inhibitors using all-atom molecular dynamics and machine learning

*Feng Zhou, Haolin Du, Weiqiang Fu, Yang Wang, and Yingsheng J. Zhang**

Beijing StoneWise Technology Co Ltd., Haidian Street #15, Haidian District, Beijing 100080, China

Abstract

We employ a combination of accelerated molecular dynamics and machine learning techniques to unravel the dynamic characteristics of CBL-B and C-CBL, and how their configurational changes conferring the binding affinity and selectivity of their ligands. We demonstrate that the activity and selectivity against CBL-B and C stem from subtle structural disparities within their binding pockets, and dissociation pathways. Our predictive model for dissociation rate constants (koff) demonstrates a moderate correlation with experimental IC50 values, effectively aligning with two available experimental koff values. Moreover, the binding free energies calculated using MM/GBSA highlight the ΔG distinction between CBL-B and C-CBL. By employing a regression strategy on dissociation trajectories, we identified key amino acids in binding pocket and along the dissociation path responsible for activity and selectivity. These amino acids are statistically significant in achieving activity and selectivity and correspond to the primary structural discrepancies between CBL-B and C-CBL. Through microsecond-scale replica exchange molecular dynamics coupled with generative model of molecular generation and ensemble docking, we accomplish comprehensive simulations of the complete apo-holo-apo transformation cycle. This approach provides an enabling first-in-class drug design technology based on apo-to-holo structure transformation.

Introduction

Casitas B-lineage lymphomas (Cbls) proteins are a group of RING finger E3 ubiquitin ligases, which contain C-CBL, CBL-B and CBL-c.[1–4] Multiple biological processes and cellular signal transduction are regulated by Cbls proteins.[5] Immune response and protein metabolism are closely related by Cbls proteins through their diverse functions.[6,7] CBL-B regulates Chimeric antigen receptor (CAR) T cell activation, immune tolerance, and has a higher activity selectively against T cell receptor complexes.[8,9] In contrast, C-CBL exhibits higher substrate affinity towards signaling proteins such as the epidermal growth factor receptor (EGFR).[10,11] The functional difference between CBL-B and C-CBL is conferred by their selective activity towards different substrates, signaling pathways, turnover rate of enzymatic kinetic property. Ubiquitination of the CBLs is effectuated by the phosphorylation of Y363 of CBL-B and Y371 of C-CBL in the highly flexible linker helix region (LHR).[12,13] The conformational changes of CBL-B and C-CBL are controlled by LHR and RING domains.[14] Moreover, the close or inactive states of CBL-B and C-CBL are

unphosphorylated and adopt an autoinhibition conformations, in which the RING and TKB domain are in close contact with each other.[12,15,16] Upon binding target substrates, E2 is recruited by RING domain, and the RING domain brings E2 in close contact with the target substrate. Meanwhile, the phosphorylation sites of CBL-B and C-CBL are exposed to corresponding kinases and the resulting phosphorylation induce a large conformational change.[12,13,17] CAR T cell therapies are vital in cancer treatment.[7,17] CBL-B as a main regulator of T cells and variety autoimmune diseases relevant cells is beneficial to corresponding therapies when its gene is knocked down, which has been shown in many experiments.[5,14] Therefore, CBL-B is a potential and significant therapeutic target. CBL-B inhibitors have gained attention as potential therapeutic agents in cancer treatment. One study showed that CBL-B inhibition using a small-molecule inhibitor enhanced antitumor immunity and improved the efficacy of immune checkpoint blockade therapy in a melanoma model[18].

The precise molecular mechanisms of Cbls proteins functions are still not fully understood. Several hypotheses have shown that selective CBL-B inhibition over C-CBL acts as a key point in solid tumor treatment.[19,20] However, high similarities in sequence and structure of CBL-B and C-CBL make the design of selective CBL-B inhibitors a daunting challenge.[7,8,17,21] CBL-B and C-CBL share high sequence homology in tyrosine kinase binding (TKB) domain, LHR and RING domain.[12–15,17,22] A study identified a few amino acids difference in the linker region between the N-terminal TKB domain and the C-terminal RING finger domain with 86% amino acid identity of CBL-B and c-CBL, respectively.[16,17] Therefore, how to exploit the little structural and sequence difference, and their subtle dynamic and kinetic differences will be crutuial to achieve selectivity. The binding affinities (Kd values) of known CBL-B inhibitors range from low micromolar to nanomolar, depending on assay conditions. There are few koff values (dissociation rates) of CBL-B inhibitors in the literature, which are key kinetic property of inhibitors. [23,24] Several strategies have been applied to design selective CBL-B inhibitors including analyzing and comparing structural difference, exploring binding pockets and targeting unique interaction by different residues between CBL-B and C-CBL. However, incorporation of kinetics via their different dissociation behavior in CBL-B drug design has not been well elaborated.

In this paper, we combine τ-random accelerated molecular dynamics (RAMD), koff prediction model and machine learning to decipher the subtle structural differences in the binding pocket and binding mode, the key amino acids for the activity and selectivity of CBL-B and C-CBL. We also complete the MD simulation for CBL-B full cycle apo-holo-apo transformation using replica exchange molecular dynamics (REMD), molecule generation technology and ensemble docking to validate our ability to identify the novel holo conformations, and demonstrate the capability to design novel holo-like drug/CBL-B complex using apo structure.

Results and discussion

1. Sequence and structure difference between CBL-B and C-CBL

The 3D structure of bound CBL-B in its inactive state (PDB ID) is shown in figure

1A, the identical amino acids between CBL-B and C-CBL are shown in red and the different ones are in blue. It is evident that CBL-B and C-CBL share the same amino acids in their binding site. However, the spatial distribution of amino acids outside of the binding pockets is not identical as show in figure 1B. Figure 1C shows the 2D structure of the bound ligand and the key amino acids around the functional groups. In these interacting amino acids, those involved in both CBL-B and C-CBL are shown in black, the ones only involved in CBL-B or C-CBL are show in red and blue respectively. Obviously, the amino acids outside of the pockets can influence binding kinetics and the ones in the dissociation pathway will have an impact on koff, which in turn contribute to selectivity and binding affinity towards to CBL-B and C-CBL.

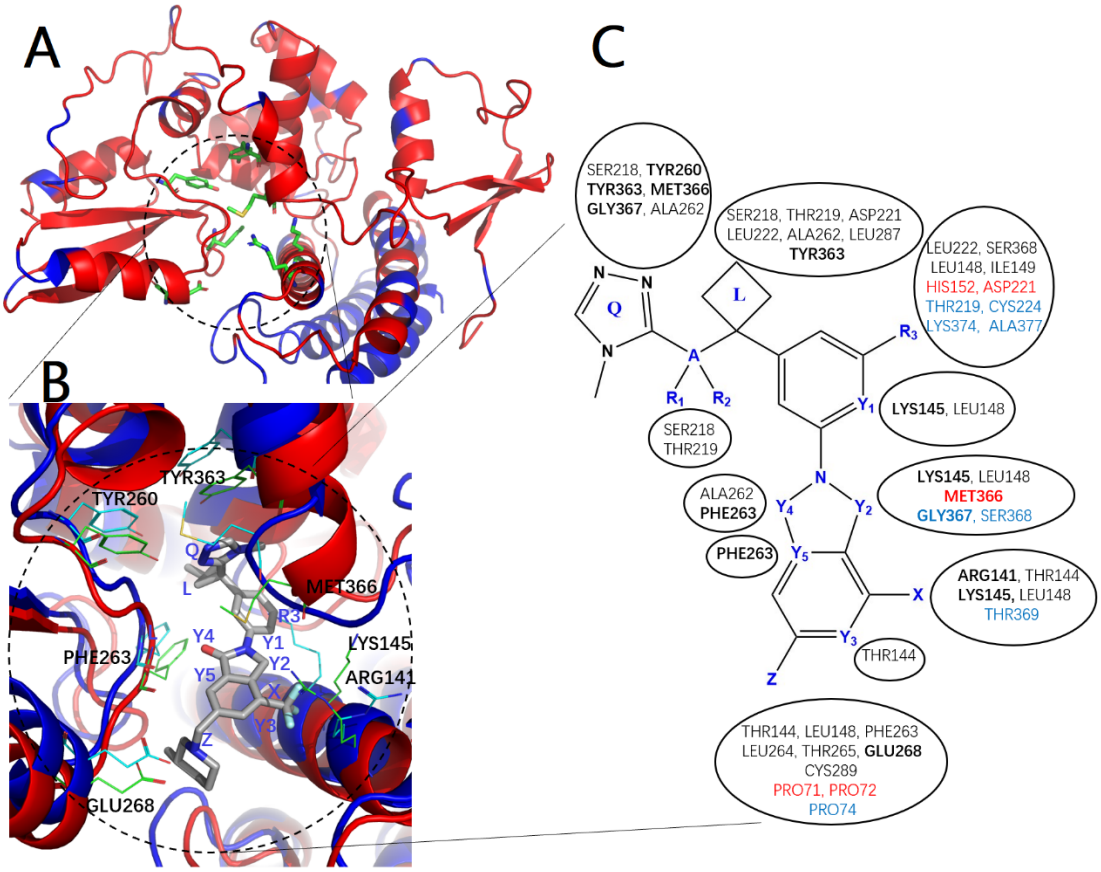

Figure 1. The cartoon representation of CBL-B protein bound with ligand with the important amino acids in the pocket show in licorice mode (PDB ID: 8GCY). (A) 3D structure of CBL-B protein, the amino acids different from C-CBL are shown in blue. (B) The cartoon representation of the pocket for CBL-B (red) and C-CBL (blue). The key amino acids are show in licorice mode with green color of carbon for CBL-B and blue color of carbon for C-CBL. (C) The 2D kekule structure of the ligand with the surrounding amino acids within 5Å far from the ligand. The amino acids involved in both CBL-B and C-CBL are shown in black, and the ones only involved in CBL-B or C-CBL are show in red and blue respectively.

In order to further analyze the structural difference between CBL-B and C-CBL in detail. We performed full-atom molecular dynamics for both CBL-B and C-CBL starting from the pdb file downloaded from RCSB (PDB ID: 8GCY and 2Y1M).

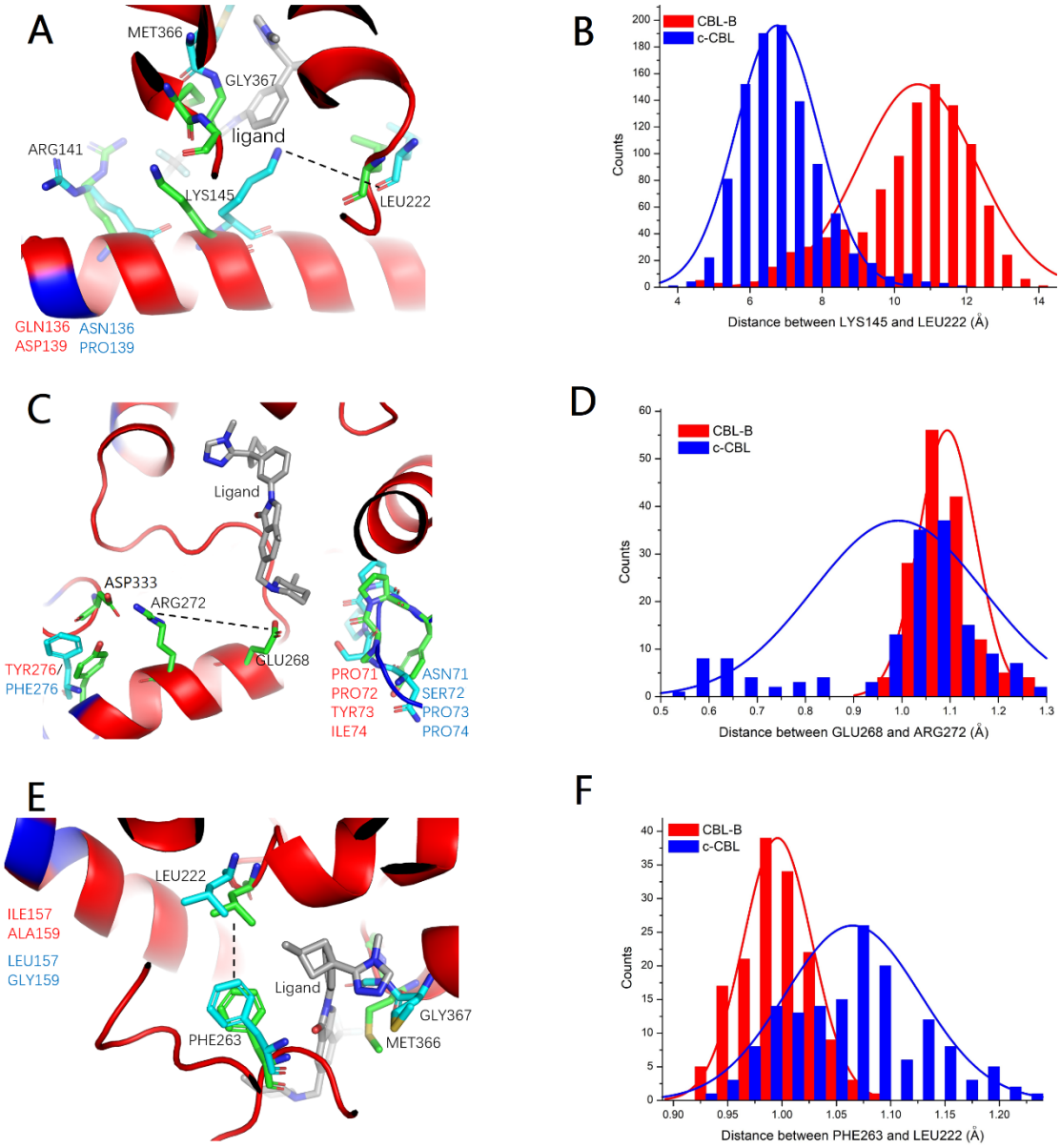

Figure 2. The cartoon representation of the local structure of the pocket for (A) LYS145 (C) GLU268 and (E) PHE263 for both CBL-B and C-CBL. The red color in the ribbon shows the same amino acids for CBL-B and C-CBL and the blue color shows the different amino acids for CBL-B and C-CBL. The key amino acids are show in licorice mode with green color of carbon for CBL-B and blue color of carbon for C-CBL. The ligand is show in black color for carbon. The distribution of the (B) LYS145-LEU222 distances, (D) GLU268-ARG272 distances, and (F) PHE263-LEU222 distances.

By analyzing the trajectory of CBL-B and C-CBL, we identified remarkable orientation discrepancy of three amino acids, LYS145, GLU268 and PHE263, in their spatial distribution in the pocket. First, LYS145 which interacts with functional groups X, Y1, Y2 of the ligand has opposite orientations for CBL-B and C-CBL. We measured the distance between LYS145 and inner residue LEU222 and found that the distance is much longer for CBL-B than for C-CBL. The longer LYS145-LEU222 distance indicates an "out" conformation of LYS145 while the shorter one indicates an "in" conformation. From Figure 2B, CBL-B has more "out" conformation of

LYS145 than C-CBL. The "out" LYS145 will have close contact with the group X (-CF3 in the case of 8GCY) of the ligand. Second, GLU268 which interacts with functional group Z of the ligand also has unique dynamic behavior for CBL-B and C-CBL. The negatively charged GLU268 has more probability to interact with positively charged ARG272 for C-CBL than for CBL-B. Although both GLU268 and ARG272 are the same for CBL-B and C-CBL, the distal amino acids are different. For example, the 276th amino acid is TYR for CBL-B and PHE for C-CBL, which leads to stronger interaction between ARG272 and the distal TYR276 and ASP333, thus weaken the interaction between ARG272 and GLU268 in CBL-B. Weakening the interaction to ARG272, GLU268 will form stronger and more stable interaction with the ligand at group Z. Third, PHE263 has stronger interaction with the deeply buried LEU222 for CBL-B than for C-CBL, which will also influence the selectivity of the ligands for CBL-B over C-CBL. We will discuss in the next paragraph in detail. Group Y2 (-CH2 in the case of 8GCY) in the ligand has close contact with MET366 in CBL-B, but with both MET366 and GLY367 in C-CBL.

2. RAMD simulation and IFPs analysis

We have discussed the different structural and dynamic behavior between CBL-B and C-CBL in the previous section based on the equilibrium molecular dynamics. To further understand the unique binding and unbinding kinetics, we performed RAMD [25,26] to study the ligand dissociation and the trajectories from which both bound states and the dissociation pathways can be analyzed. We collected 49 ligands with various activity and selectivity from patents from NURIX[27,28], HOTSPOT[29,30], GENTECH[31,32], NIMBUS[33,34] and XIANSHENG.[35,36] The ligands were prepared using RDKIT[37] and docked into the binding pocket using LEDOCK[38]. For each ligand, 90 independent RAMD were performed based on six different initial structures from 10ns normal MD. The interaction finger prints (IFPs) along the dissociation pathway were obtained from the RAMD trajectories and the linear regression is used to determine the key amino acids which influence activity or selectivity.

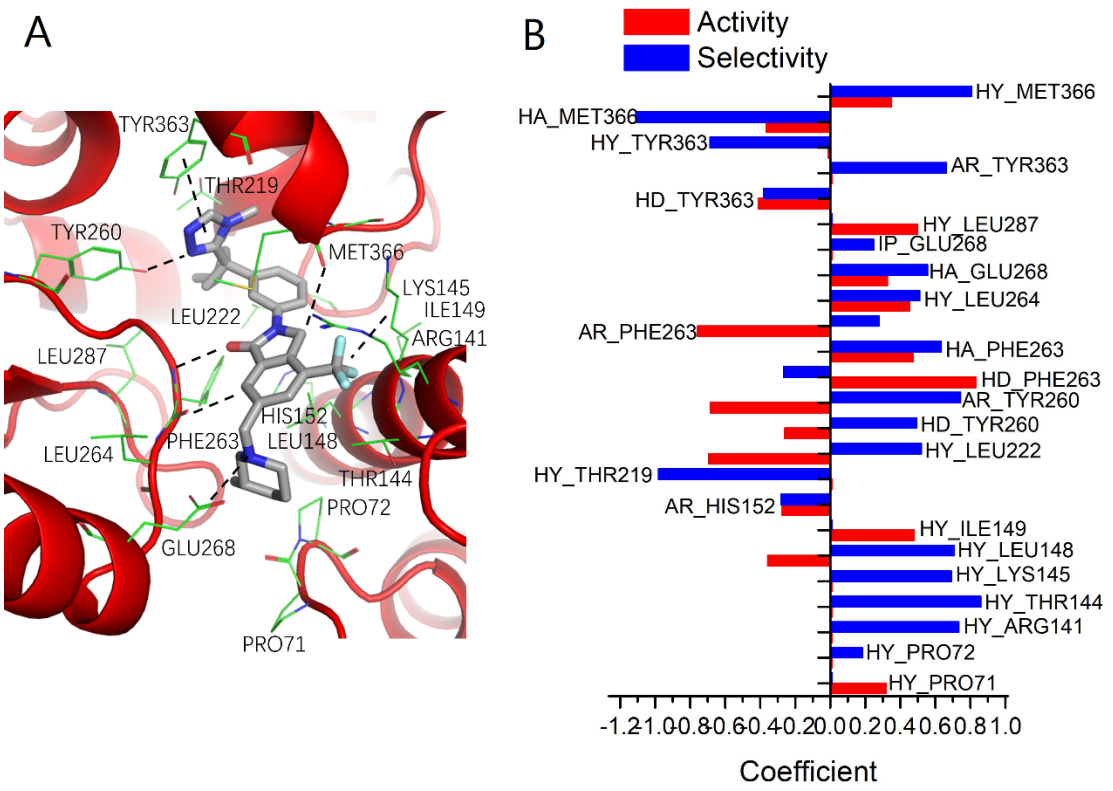

Figure 3. The key amino acids in the binding pocket and their importance in activity and selectivity. (A) The position of the amino acids (carbon in green) in the pocket. The carbons of the reference ligand are in black (B) The LR coefficient of top-ranked amino acids which has most impact on the activity (red color) or selectivity (blue color).

From figure 3, we identified the key IFPs contributing to the activity or selectivity. For example, HY_ILE149, HD_PHE263, HA_PHE263, HY_LEU264, HA_GLU268, HY_LEU287, HY_MET366 have positive impact on the activity. HY_ARG141, HY_THR144, HY_LYS145, HY_LEU148, HY_LEU222, HD_TYR260, AR_TYR260, HA_PHE263, AR_PHE263, HY_LEU264, HA_GLU268, IP_GLU268, AR_TYR363, HY_MET366 influence selectivity. Several IFPs which both enhance activity and selectivity are HA_PHE263, HY_LEU264, HA_GLU268 and HY_MET366. LYS145, PHE263 and GLU268 which has influence on the selectivity have also been identified previously when analyzing the different structural and dynamic behaviors between CBL-B and C-CBL. In detail, the functional group X has stronger interaction with LYS145 in “out” conformation as in CBL-B. Functional group Z has stronger salt bridge interaction with GLU268 in CBL-B than C-CBL. Hydrogen bond donor of PHE263 has positive impact on selectivity but negative impact on activity. An example is the ligand from NIMBUS, in which the carbonyl group at Y_4 is replaced by nitrogen to increase the selectivity but at the price of losing some activity. Amino acids 71 to 74 are different for CBL-B and C-CBL, especially PRO71 and PRO72, though far from the binding pocket has positive impact on the activity and selectivity respectively through dynamic perturbation.

3. koff prediction and MM/GBSA calculation

After discussion on the impact of sequence and structure difference of CBL-B and C-CBL to activity and selectivityfrom in the view of equilibrium and non-equilibrium molecular dynamics. Next we shift our focus on the contribution of binding free energy (ΔG) and kinetic dissociation rate (koff) to their activity and selectivity. Applying our ML koff prediction model[39], we predicted the koff values of 49 CBL-B ligands. The predicted koff values are highly correlated (Pearson correlation coefficient r_P is 0.71) with the simulated koff values from RAMD for these ligands (fig in suppl). To further validate our results, we compared the predicted koff with the experimental data. We examined two patents which published the experiment retention time (1/koff) using the SPR experiments from NURIX[23] and HOTSPOT[24]. The experimental retention time is 90~180 s for NURIX ligand series, and 10^4 s for HOTSPOT series. For comparison, our predicted RT is in the range of 40~315s for NURIX ligand series and 0.6~1.2x10^4 s for HOTSPOT series, which match well with the experimental data. Because lack of enough experimental koff data for CBL-B inhibitors, we also used the experimental pIC50 instead to compare with the predicted koff values. We observed the -log(koff) has some correlation with the experiment pIC50, the Pearson correlation coefficient r_P is 0.48. (suppl) Considering the r_P between experimental pkD and pkoff is 0.68,[40] and the r_P between predicted and experimental -log(koff) is 0.73 as reported in our previous work[39], so the 0.48 correlation coefficient between predicted -log(koff) and pIC50 (IC50≈kD) is acceptable. From this point of view, the predicted koff can be used to evaluate the activity.

To understand how the koff or the dissociation pathway are associated with the selectivity, we applied IFP analysis derived from the dissociation trajectories from 49 ligands as show in figure 3. Here we present one case to elaborate how the koff influences the selectivity. We plot the IFP composition along the dissociation pathway of ligands from HOTSPOT patent (refs) for CBL-B and C-CBL, as shown in figure 4.

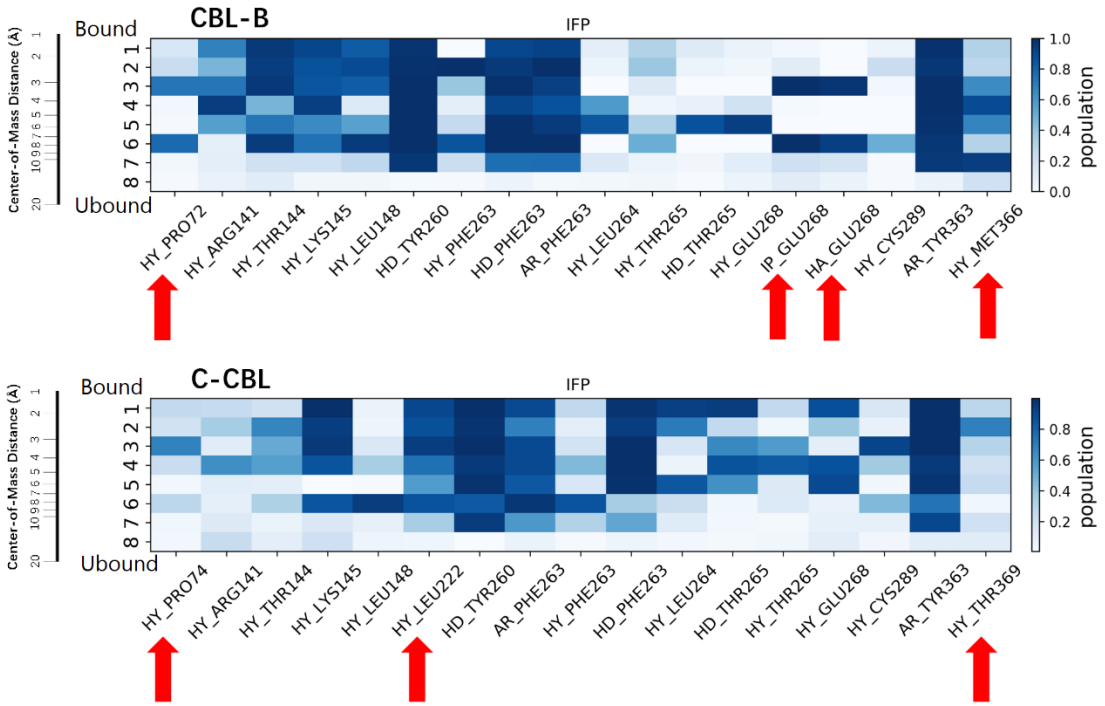

Figure 4. A representative visualization of interaction fingerprints (IFP) composition along the dissociation pathway of ligand of CBL-B and C-CBL. Cluster 1 is the bound state, and Cluster 8 is the unbound state. The key amino acids make the difference for CBL-B and C-CBL were indicated by red arrow.

From figure 4, we identified some impactful amino acids along the dissociation pathway. For example, HY_MET366 has strong interaction with the ligand for CBL-B until the full dissociation while for C-CBL, it's HY_THR369 instead whose interaction is much weaker. Both HA_GLU268 and IP_GLU268 contribute to the binding and increase the retention time of ligand in CBL-B, but they are absent for C-CBL. At the entrance of the pocket, PRO72 has hydrophobic interaction with the ligand in CBL-B, but this interaction comes from PRO74 for C-CBL and it is weaker. All these effects lead to longer retention time for ligand in CBL-B than C-CBL. The simulated -log(koff) is 2.33 for CBL-B and 1.78 for C-CBL.

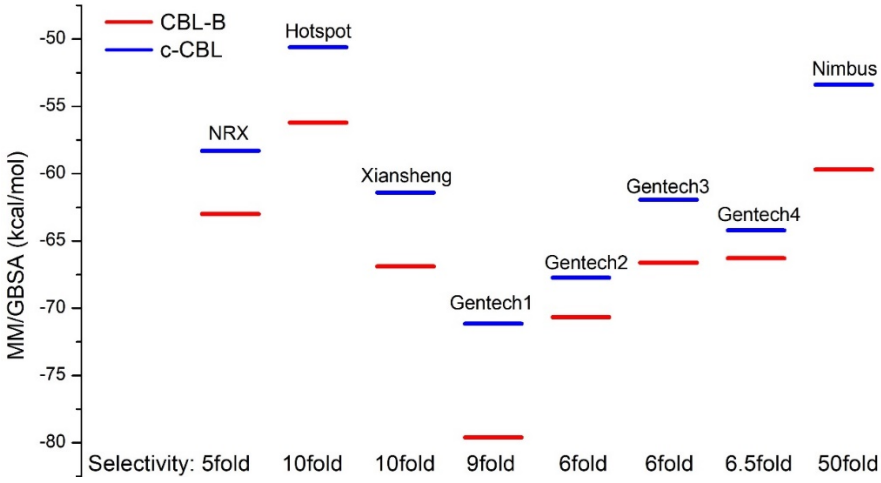

(或者换成table)

Figure 5: The calculated binding free energy between CBL-B and ligand (red), and between C-CBL and ligand (blue). The selectivity for each ligand is shown below.

On the other hand, we also calculated the binding free energy using MM/GBSA method ([41]) using gmx_PBSA script[42] for ligands with high selectivity, as shown in figure 5. As can be seen, these highly selective ligands differ significantly in their calculated ΔG for CBL-B and C-CBL. The ΔΔG between CBL-B and C-CBL is in the range of 2~9 kcal/mol, in consistent with their respective koff values. These results indicate the kinetic properties are the differentiator of selectivity and binding affinity in CBL-B and C-CBL.

4. Ensemble docking and REMD

In following section, we discuss the procedure of research from a first-in-class point of view. That's imaging we start without the cocrystal structure or from apo structure to design holo-structure-based ligands.

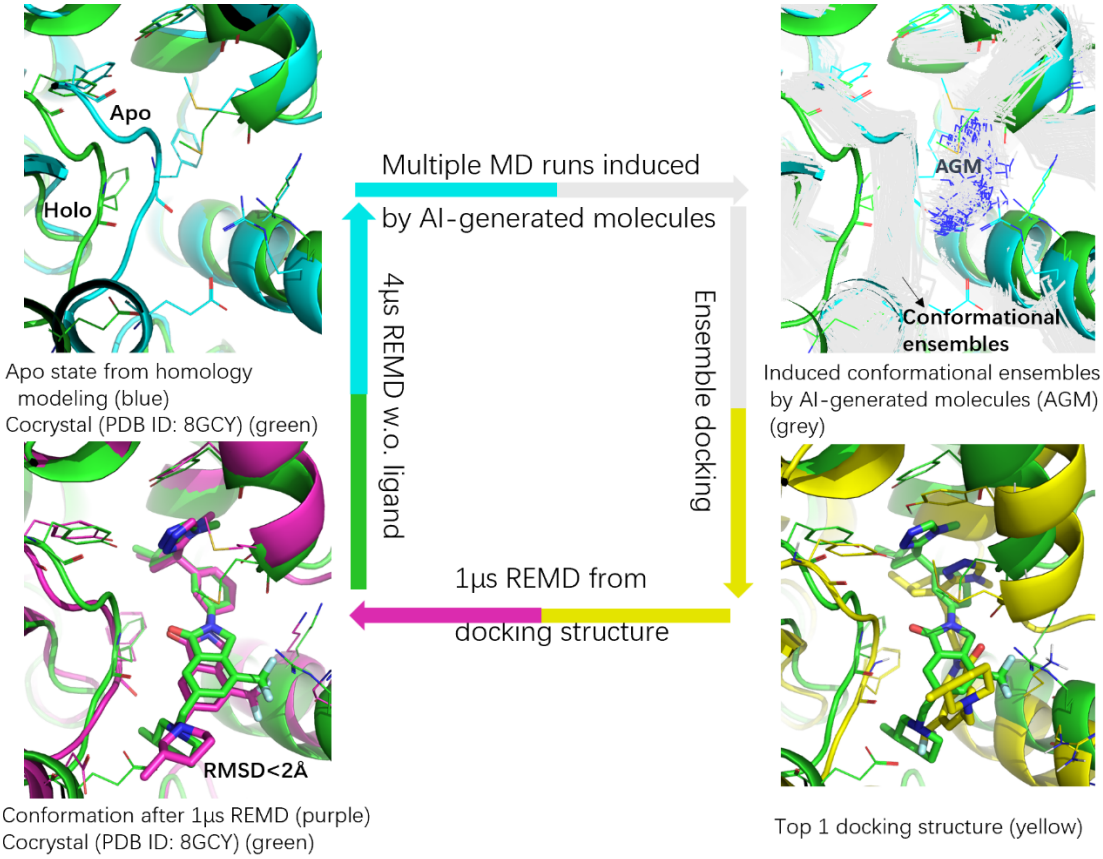

Figure 6.

As shown in figure 6, we first retrieved the native apo structure of C-CBL from RCSB website. We then build our homology-model CBL-B structure using I-TASSER server.[43] This homology-modeled CBL-B structure is an apo state and all docking efforts for known CBL-B inhibitors failed due to the undruggable narrow pocket of apo conformation. Applying electronic density-based generative molecule generation methods[44], we obtained 24 AI-generated molecules (AGM) from this narrow pocket of the apo CBL-B structure and run 3x24 100ns MD to generate the induced conformational ensembles of CBL-B. Then, we applied proprietary ensemble docking protocol on the ligand from the cocrystal (PDB ID: 8GCY) and used the clustering method to obtain the first ranked docking pose. Based on this docking pose, we performed 1μs replica exchange MD (REMD) using 16 replicas in which the temperature ranged from 290K to 490K (total 16μs). The conformation by clustering the trajectory at 300K has RMSD less than 2A from the cocrystal structure, the holo structure of CBL-B. Lastly, we removed the ligand and ran another 4μs REMD using 16 replicas (total 64μs), the CBL-B conformation reverted to the apo state. Therefore, we build a full cycle of apo to holo then to apo using molecular generation, ensemble docking and long time REMD. Our overall procedure validates the feasibility of AI and simulation based de novo first-in-class drug design.

Conclusion

In silico drug design from apo structures to give diverse drug-like molecules compatible to holo-conformations is a continuous challenge in drug discovery process. We integrate accelerated molecular dynamics and machine learning techniques to elucidate the distinct structural and kinetic attributes of CBL-B and C-CBL to their binding modes and selectivity against diverse ligands. These variances in activity and selectivity stem from nuanced disparities within the binding pocket's structure influenced by distal residues outside of the pocket through kinetic and dynamic perturbation via binding and the trajectory of dissociation.

Our predictive model for koff exhibits a moderate correlation with experimental IC50 values, closely aligning with both experimental koff datasets. MM/GBSA binding free energy calculation reveals the discernible ΔG variation between CBL-B and C-CBL even though they share identical amino acids in their binding pockets. Key amino acids responsible for activity and selectivity along the dissociation path are identified through a regression strategy applied to multiple dissociation trajectories. These amino acids correspond to the principal structural divergence between CBL-B and C-CBL. We applied ms-scale replica exchange MD in conjunction with generative molecular generation models and ensemble docking to achieve a comprehensive simulation of the complete apo-holo-apo transformation cycle. This approach provides a valid approach for first-in-class drug design from apo to holo complexes.

Reference

(1) Swaminathan, G.; Tsygankov, A. Y. The Cbl Family Proteins: Ring Leaders in Regulation of Cell Signaling. *Journal of Cellular Physiology*. October 2006, pp 21–43. https://doi.org/10.1002/jcp.20694.

(2) Deshaies, R. J.; Joazeiro, C. A. P. RING Domain E3 Ubiquitin Ligases. *Annual Review of Biochemistry*. 2009, pp 399–434. https://doi.org/10.1146/annurev.biochem.78.101807.093809.

(3) Joazeiro, C. A. P.; Wing, S. S.; Huang, H. K.; Leverson, J. D.; Hunter, T.; Liu, Y. C. The Tyrosine Kinase Negative Regulator C-Cbl as a RING-Type, E2- Dependent Ubiquitin-Protein Ligase. *Science (1979)* **1999**, *286* (5438), 309–312. https://doi.org/10.1126/science.286.5438.309.

(4) Shao, Y.; Yang, C.; Elly, C.; Liu, Y. C. Differential Regulation of the B Cell Receptor-Mediated Signaling by the E3 Ubiquitin Ligase Cbl. *Journal of Biological Chemistry* **2004**, *279* (42), 43646–43653. https://doi.org/10.1074/jbc.M404082200.

(5) Duda, D. M.; Scott, D. C.; Calabrese, M. F.; Zimmerman, E. S.; Zheng, N.; Schulman, B. A. Structural Regulation of Cullin-RING Ubiquitin Ligase Complexes. *Current Opinion in Structural Biology*. April 2011, pp 257–264. https://doi.org/10.1016/j.sbi.2011.01.003.

(6) *Ubiquitin Ligase Activity and Tyrosine Phosphorylation Underlie Suppression of Growth Factor Signaling by C-Cbl/Sli-1*.

(7) Kales, S. C.; Ryan, P. E.; Nau, M. M.; Lipkowitz, S. Cbl and Human Myeloid Neoplasms: The Cbl Oncogene Comes of Age. *Cancer Research*. June 15, 2010, pp 4789–4794. https://doi.org/10.1158/0008-5472.CAN-10-0610.

(8) Chiang, Y. J.; Kole, H. K.; Brown, K.; Naramura, M.; Fukuhara, S.; Hu, R.-J.; Jang, I. K.; Gutkind, J. S.; Shevach, E.; Gu, H. Cbl-b Regulates the CD28 Dependence of T-Cell Activation. *Nature* **2000**, *403* (6766), 216–220. https://doi.org/10.1038/35003235.

(9) Qiao, G.; Li, Z.; Molinero, L.; Alegre, M.-L.; Ying, H.; Sun, Z.; Penninger, J. M.;

Zhang, J. T-Cell Receptor-Induced NF-KB Activation Is Negatively Regulated by E3 Ubiquitin Ligase Cbl-b. *Mol Cell Biol* **2008**, *28* (7), 2470–2480. https://doi.org/10.1128/mcb.01505-07.
(10) Thien, C. B. F.; Walker, F.; Langdon, W. Y. *RING Finger Mutations That Abolish C-Cbl-Directed Polyubiquitination and Downregulation of the EGF Receptor Are Insufficient for Cell Transformation*; 2001; Vol. 7.
(11) Mueller, D. L. E3 Ubiquitin Ligases as T Cell Anergy Factors. *Nature Immunology*. September 2004, pp 883–890. https://doi.org/10.1038/ni1106.
(12) Kassenbrock, C. K.; Anderson, S. M. Regulation of Ubiquitin Protein Ligase Activity in C-Cbl by Phosphorylation-Induced Conformational Change and Constitutive Activation by Tyrosine to Glutamate Point Mutations. *Journal of Biological Chemistry* **2004**, *279* (27), 28017–28027. https://doi.org/10.1074/jbc.M404114200.
(13) Yang, T.; Han, L.; Huo, S. Dynamics and Allosteric Information Pathways of Unphosphorylated C-Cbl. *J Chem Inf Model* **2022**, *62* (23), 6148–6159. https://doi.org/10.1021/acs.jcim.2c01022.
(14) Dou, H.; Buetow, L.; Hock, A.; Sibbet, G. J.; Vousden, K. H.; Huang, D. T. Structural Basis for Autoinhibition and Phosphorylation-Dependent Activation of c-Cbl. *Nat Struct Mol Biol* **2012**, *19* (2), 184–192. https://doi.org/10.1038/nsmb.2231.
(15) Dou, H.; Buetow, L.; Hock, A.; Sibbet, G. J.; Vousden, K. H.; Huang, D. T. Structural Basis for Autoinhibition and Phosphorylation-Dependent Activation of c-Cbl. *Nat Struct Mol Biol* **2012**, *19* (2), 184–192. https://doi.org/10.1038/nsmb.2231.
(16) Peschard, P.; Kozlov, G.; Lin, T.; Mirza, I. A.; Berghuis, A. M.; Lipkowitz, S.; Park, M.; Gehring, K. Structural Basis for Ubiquitin-Mediated Dimerization and Activation of the Ubiquitin Protein Ligase Cbl-b. *Mol Cell* **2007**, *27* (3), 474–485. https://doi.org/10.1016/j.molcel.2007.06.023.
(17) Designed Research; Y, F. I. K.; Performed Research; Y, M. Y. K.; Pnas I, A. Autoinhibition and Phosphorylation-Induced Activation Mechanisms of Human Cancer and Autoimmune Disease-Related E3 Protein Cbl-b. **2011**, *108*. https://doi.org/10.1073/pnas.1110712108/-/DCSupplemental.
(18) Gavali, S.; Liu, J.; Li, X.; Paolino, M. Ubiquitination in T-Cell Activation and Checkpoint Inhibition: New Avenues for Targeted Cancer Immunotherapy. *International Journal of Molecular Sciences*. MDPI October 1, 2021. https://doi.org/10.3390/ijms221910800.
(19) Identification of the Selective CBL-b Inhibitors Which Effectively Prevent T Cells from Exhaustion and Demonstrate Synergistic Anti-Tumor Activity in Combination with an Anti-PD1 Antibody.
(20) Thien, C. B. F.; Langdon, W. Y. C-Cbl and Cbl-b Ubiquitin Ligases: Substrate Diversity and the Negative Regulation of Signalling Responses. *Biochemical Journal*. October 15, 2005, pp 153–166. https://doi.org/10.1042/BJ20050892.
(21) Blaquiere, N.; Villemure, E.; Staben, S. T. Medicinal Chemistry of Inhibiting RING-Type E3 Ubiquitin Ligases. *Journal of Medicinal Chemistry*. American Chemical Society August 13, 2020, pp 7957–7985. https://doi.org/10.1021/acs.jmedchem.9b01451.
(22) Buetow, L.; Tria, G.; Ahmed, S. F.; Hock, A.; Dou, H.; Sibbet, G. J.; Svergun, D. I.; Huang, D. T. Casitas B-Lineage Lymphoma Linker Helix Mutations Found in Myeloproliferative Neoplasms Affect Conformation. *BMC Biol* **2016**, *14* (1). https://doi.org/10.1186/s12915-016-0298-6.
(23) WO2019148005A1 (Nurix).
(24) POSTER-HotSpot-Therapeutics_SITC_2021.
(25) Kokh, D. B.; Amaral, M.; Bomke, J.; Grädler, U.; Musil, D.; Buchstaller, H. P.; Dreyer, M. K.; Frech, M.; Lowinski, M.; Vallee, F.; Bianciotto, M.; Rak, A.; Wade, R. C. Estimation of Drug-Target Residence Times by τ-Random Acceleration Molecular Dynamics Simulations. *J Chem Theory Comput* **2018**, *14* (7), 3859–3869. https://doi.org/10.1021/acs.jctc.8b00230.
(26) Kokh, D. B.; Doser, B.; Richter, S.; Ormersbach, F.; Cheng, X.; Wade, R. C. A Workflow for Exploring Ligand Dissociation from a Macromolecule: Efficient Random Acceleration Molecular Dynamics Simulation and Interaction Fingerprint Analysis of Ligand Trajectories. *Journal of Chemical Physics* **2020**, *153* (12). https://doi.org/10.1063/5.0019088.

(27) Whelan, S.; Karim, C.; Ye, J.; Ingallinera, T.; Cherala, G.; Jameson, K.; Williams, A.; Sharp, A.; Krebs, M.; Pacey, S.; Blagden, S.; Plummer, R.; Hochhauser, D.; Evans, J.; Bono, J. De; Powers, J. 777 Initial Clinical Characterization of Novel Proximal Biomarkers for NX-1607, a First-in-Class Oral CBL-B Inhibitor, in Patients with Advanced Malignancies; BMJ, 2022; pp A808–A808. https://doi.org/10.1136/jitc-2022-sitc2022.0777.
(28) Gallotta, M.; Gosling, J.; Tenn-McClellan, A.; Ranucci, S.; Romo, J. G.; Cohen, F.; Hansen, G.; Sands, A.; Guiducci, C.; Rountree, R. 824 NX-1607, a Small Molecule Inhibitor of the CBL-B E3 Ubiquitin Ligase, Promotes T and NK Cell Activation and Enhances NK-Mediated ADCC in a Mouse Lymphoma Tumor Model; BMJ, 2022; pp A859–A859. https://doi.org/10.1136/jitc-2022-sitc2022.0824.
(29) Qi, Y.; Kuai, J.; Bi, Y.; Sun, H.; Jaeger, S.; Greco, D.; Carson, K.; Reilly, T.; Harriman, G.; Wang, F. 424 An Allosteric, Orally Administered CBL-B Inhibitor Remodels the Tumor Microenvironment and Enhances Immune-Mediated Tumor Growth Inhibition; BMJ, 2022; pp A445–A445. https://doi.org/10.1136/jitc-2022-sitc2022.0424.
(30) Kuai, J.; Bi, Y.; Qi, Y.; Conrady, D.; Govindaraj, R.; Hone, G.; Aldrin Denny, R.; Carson, K.; Harriman, G.; Wang, F. 864 Identification of a Novel Allosteric Oral Cbl-b Inhibitor That Augmented T Cell Response and Enhanced NK Cell Killing in Vitro and in Vivo. *J Immunother Cancer* **2021**, *9* (Suppl 2), A905–A905. https://doi.org/10.1136/jitc-2021-sitc2021.864.
(31) Sabnis, R. W. Novel Lactams as Cbl-b Inhibitors for Treating Cancer. *ACS Med Chem Lett* **2022**, *13* (10), 1556–1557. https://doi.org/10.1021/acsmedchemlett.2c00413.
(32) WO2022169997A1.
(33) WO2022272248A1.
(34) WO2022217276A1.
(35) WO2023072273A1.
(36) WO2023036330A1.
(37) Landrum, G. RDKit Documentation (2019.09.1). *Https://Www.Rdkit.Org/* **2019**.
(38) Wang, Z.; Sun, H.; Yao, X.; Li, D.; Xu, L.; Li, Y.; Tian, S.; Hou, T. Comprehensive Evaluation of Ten Docking Programs on a Diverse Set of Protein-Ligand Complexes: The Prediction Accuracy of Sampling Power and Scoring Power. *Physical Chemistry Chemical Physics* **2016**, *18* (18), 12964–12975. https://doi.org/10.1039/c6cp01555g.
(39) Zhou, F.; Yin, S.; Xiao, Y.; Lin, Z.; Fu, W.; Zhang, Y. J. Structure-Kinetic Relationship for Drug Design Revealed by a PLS Model with Retrosynthesis-Based Pre-Trained Molecular Representation and Molecular Dynamics Simulation. *ACS Omega* **2023**, *8* (20), 18312–18322. https://doi.org/10.1021/acsomega.3c02294.
(40) Amangeldiuly, N.; Karlov, D.; Fedorov, M. V. Baseline Model for Predicting Protein-Ligand Unbinding Kinetics through Machine Learning. *J Chem Inf Model* **2020**, *60* (12), 5946–5956. https://doi.org/10.1021/acs.jcim.0c00450.
(41) Kollman, P. A.; Massova, I.; Reyes, C.; Kuhn, B.; Huo, S.; Chong, L.; Lee, M.; Lee, T.; Duan, Y.; Wang, W.; Donini, O.; Cieplak, P.; Srinivasan, J.; Case, D. A.; Cheatham, T. E. Calculating Structures and Free Energies of Complex Molecules: Combining Molecular Mechanics and Continuum Models. *Acc Chem Res* **2000**, *33* (12), 889–897. https://doi.org/10.1021/ar000033j.
(42) Valdés-Tresanco, M. S.; Valdés-Tresanco, M. E.; Valiente, P. A.; Moreno, E. Gmx_MMPBSA: A New Tool to Perform End-State Free Energy Calculations with GROMACS. *J Chem Theory Comput* **2021**, *17* (10), 6281–6291. https://doi.org/10.1021/acs.jctc.1c00645.
(43) Yang, J.; Zhang, Y. I-TASSER Server: New Development for Protein Structure and Function Predictions. *Nucleic Acids Res* **2015**, *43* (W1), W174–W181. https://doi.org/10.1093/nar/gkv342.
(44) Ding, K.; Yin, S.; Li, Z.; Jiang, S.; Yang, Y.; Zhou, W.; Zhang, Y.; Huang, B. Observing Noncovalent Interactions in Experimental Electron Density for Macromolecular Systems: A Novel Perspective for Protein-Ligand Interaction Research. *J Chem Inf Model* **2022**, *62* (7), 1734–1743. https://doi.org/10.1021/acs.jcim.1c01406.